Light fragment emission as studied by the (p,pHe) reactions on Be and Ag with 300 MeV protons

R. G. Korteling, R. E. L. Green,* and J. M. D'Auria
Chemistry Department, Simon Fraser University, Burnaby, British Columbia, Canada V5A 1S6

R. L. Helmer and K. P. Jackson
TRIUMF, Vancouver, British Columbia, Canada V6T 2A3

S. B. Kaufman and B. D. Wilkins
Physics Division, Argonne National Laboratory, Argonne, Illinois 60439
(Received 26 October 1989)

Inclusive and exclusive differential cross sections have been measured for the (p,pHe) reaction on Be and Ag with 300 MeV protons. Detectors in coplanar geometry were used to measure singles spectra and coincidence spectra between protons and He isotopes. The particle spectra are surprisingly similar between the inclusive and exclusive measurements as well as between the two widely different targets. The proton differential mean multiplicities associated with He emission show significant structure as a function of He emission angles except for the case of low energy emission from Ag. An analysis of the data in terms of rapidity and relativistically invariant cross section is in general agreement with the notion of isotropic emission from a moving source for the He isotopes from both targets. Only in extreme kinematic regions, where events were selected in which momentum in excess of 300 MeV/c was transferred to the target system, did the contours become nonspherical. The mass of the emitting source is shown to be small. The results are consistent with the concept of deexcitation of a small excited source by effective binary breakup leading to fragment emission.

I. INTRODUCTION

Intermediate energy complex reactions are generally considered to proceed through a stage in which a form of equilibrium is reached. The hot pseudoequilibrated zone of the nucleus is believed to subsequently cool and deexcite by expansion and the emission of particles and fragments in a statistical manner. This hot spot is believed to dictate the particle and excited-state distributions of the emitted fragments.[1-3] Such a mechanism permits some simplicity in the formalism used to describe these reactions and a number of recent calculations are based on this model.[4-9] In fact, comparisons to the big bang, with its time evolution and freeze out temperatures, etc., are made and similar formalisms are sometimes used.[1,10] An added incentive to study such systems is that if such a state were to be formed, the equation of state could be studied for regions of nuclear matter at high temperature or densities.[11-15]

However, it is still to be conclusively demonstrated that such a state is routinely formed or what its characteristics are. Whereas the majority of the inclusive measurements are consistent with such a state, they involve model-dependent or average interpretations. What is worse, a wide variety of models, based on widely differing assumptions, have yielded similar agreement with the data.[16] There is also some question whether this state is in equilibrium in all senses or whether it is in equilibrium in some aspects and not in others. The reaction could proceed through thermal equilibrium but not chemical or be in equilibrium in some reactions and not in others. The problem is that in most intermediate and high energy complex reactions a true amalgamation of projectile and target is not reached. It is therefore important to determine when it is valid to describe the reaction as proceeding through an equilibrated state and when it is not and this needs to be answered for a wide range of reaction conditions.

A major effort to characterize an assumed equilibrated emitting source by the technique of measuring particle correlations has been undertaken, mainly for heavy-ion reactions. The size of the emitting source is determined from the particle interferometry and its temperature from a measurement of the distribution of fragment excited states.[17-21] The results are consistent with a source size which is a function of the emitted particle sizes and with a source density of about half normal nuclear matter. The particle excited-state measurements give a temperature of about 5 MeV whereas the spectra of the emitted fragments suggest a much higher value. This discrepancy is explained by suggesting that the reaction proceeds through stages where the fragment kinetic-energy distribution is determined at an early stage followed by chemical equilibrium. Complementary measurements of the gamma decay of selected fragments has generally given a somewhat lower temperature.[22] The difference is blamed on the difficulty of accurately determining the feeding of the measured states from higher-lying states.

Several heavy-ion studies, observing single-particle inclusive emission as well as two-particle correlations, have also investigated the nature of the emitting source.[23-27] Although they all are in the incident energy range of

20–50 MeV/nucleon and therefore at much lower incident velocities than this study, their total beam energies are comparable. Covering a wide range of target projectile combinations, the results are generally consistent with the formation of two or three sources which are subsets of the target projectile combination. A low rapidity targetlike source with low temperatures in the range of 3.5–5 MeV is clearly separate from a higher rapidity projectilelike source with a higher temperature. An intermediate source is also seen with even higher temperatures. The separate roles of target and projectile, and therefore sources, is clearly seen in these reactions.

A recent study[28] using protons on the very different Be and Ag targets has shown that the sizes and temperatures of the emitting source are the same for both targets and equivalent to those measured in the heavy-ion reactions. Furthermore, the source sizes were a strong function of the measured correlation particles, where small sizes came from systems with known excited states and large sizes came from systems without such states. These results led the authors to question whether these types of measurements are indicative of the emitting source or rather a measure of final-state interactions.

The inferred source temperatures from the correlation studies are in general agreement with the concept of limiting temperatures and the initial measurements of the value for intermediate energy heavy-ion reactions.[29–31] This limiting temperature concept is, in turn, used to argue that phase changes are occurring with the increased excitation energy being used to increase the degrees of freedom of the system and not its temperature. However, Wada *et al.*[31] have noted that the Fermi gas model in its simplest form predicts an average excitation per nucleon of about 8 MeV for this temperature and that the measured limit in temperature may simply be a reflection of the limit of the binding energy in nuclei.

It has been shown for intermediate energy proton-induced inclusive reactions that the majority of the fragment emission cross section can be explained by statistically emitting sources much smaller than the total target nucleus and that these sources have velocities in the lab directly proportional to the radial velocity of the emitted fragment.[32,33] The use of the proton projectile has restricted the source formation to the target system, but not necessarily to a single source, as opposed to the case for heavy-ion reactions mentioned above. The proposal of a continuum of sources is similar to the speculation by Remington *et al.*[25] that a small, hot source evolves into a cooler, large targetlike source as a means to explain their analysis of neutron fragment coincidences from ^{14}N plus Ho and Ni reactions. Although these proposed statistically emitting sources support the concept that the reaction proceeded through a state of thermal equilibrium, it does not mean that chemical equilibrium was also attained. In fact, Boal has calculated that chemical equilibrium is not reached in all cases.[10] When more exclusive measurements are made on simple systems by studying the $(p,2p)$ and (p,pd) reactions on Be, the reaction seems to be dominated by direct interaction components.[34,35] There must be a transition in the dominance of the reaction mechanisms between this very simple case and the more normal complex reaction conditions.

This study is designed to probe the limits of the conventional concept of intermediate energy complex reactions. An extensive set of data was collected where the emission of light fragments, mainly H and He isotopes, was measured in coincidence with other particles, mainly a high energy proton believed to be the incident projectile in most cases. Both Be and Ag targets were bombarded with 300 MeV protons in an effort to compare a relatively simple system, Be, with a complex system, Ag. A rather complete angular distribution was measured in both singles and coincident modes. By selecting on the coincident high energy proton, some selection on the emitting source could be made. A study of the correlated fragment emission is analyzed in terms of the expected energy and angular dependence for direct versus statistical emission to determine where one or the other process dominates.

Of the many facets which could be presented, this paper will restrict itself to dealing with the emission of the He isotopes in singles and in coincidence with high energy protons.

II. EXPERIMENTAL TECHNIQUES

The experimental work was conducted using a 25 cm radius scattering chamber located in the 4*B* beam line of the TRIUMF accelerator. The electronics and data acquisition computer were located in an equipment trailer approximately 50 m away. The main off-line data analysis was performed at the Simon Fraser University Computer Center. Some of the experimental techniques have been described in previous publications[32,34,36] and will not be discussed in detail here. The new aspects associated with this experiment will be presented in greater detail.

A. Beam, target, chamber, and detectors

Incident 300 MeV unpolarized protons were chosen so that the full energy protons could be stopped in detectors of reasonable size and response functions and yet provide sufficient fragment yields for the measurements to be made. Previous results[36] have indicated that the incident energy had no significant effect on the general fragmentation process except for a general increase in cross section with beam energy. At this energy the beam characteristics were sufficient for the measurements to be made using detectors in close geometry. The beam spot was mainly within a 2–3 mm diam area centered to within 2 mm. The beam halo was reduced to the point that target-in versus target-out singles rates in all detectors exceeded 10 to 1 and in many cases, reached 100 to 1. The beam current was adjusted between 5 and 20 nA to keep the singles rates in all detectors well within their linear operating ranges.

The two targets used in this experiment were commercially prepared free standing foils of Be and Ag with mean thicknesses of 2.26 and 2.16 mg/cm^2, respectively. They were positioned 45° to the beam to minimize target thickness corrections which were significant only for the

He and heavier isotopes. A standard half-target thickness correction was made for each case. No light mass target impurity effects were observed for the measured fragments, such as resulting from oxide layers.

The scattering chamber was specially constructed to allow for the measurement of low energy H isotopes and all heavier elements in the beam line vacuum while measuring the high energy H isotopes with detectors located outside the chamber. Thin walled hemispherical domes of 860 mg/cm^2 Al and with a 25 cm radius were connected to a center ring forming a near spherical chamber. The center ring subtended approximately 12° on either side of the beam and restricted external measurements to within 12° to 168° on either side of the beam.

A schematic representation of the experimental arrangement is given in Fig. 1. Standard surface barrier Si detector telescopes (30, 500, and 2000 μm followed by a veto detector) were mounted on a 15 cm radius at six angles ($-30°$, $-60°$, $\pm 90°$, $-120°$, $-150°$). The angular sign convention that has been adopted in this paper is to refer to positive angles as being on the same side of the beam as a coincident proton or fragment trigger and negative angles being on the opposite side. The first three detectors in each telescope were nominally 100 mm^2 active area and the reject detector was 150 mm^2. No passive collimators were used because high energy protons were actively collimated by these same detectors. In such a case, the solid angle for each fragment depends on the detectors involved in its detection and was ≈ 4 msr for these telescopes. Behind each Si detector telescope and external to the chamber, a high energy proton detector was positioned to measure the same angular emission as the Si detectors. These were either $10 \times 10 \times 20$ cm NaI or 15 cm diam by 76 cm plastic scintillators, both preceded by 0.6 cm thick ΔE scintillators. A large 30 cm diam by 76 cm plastic scintillator with a 15 cm diam ΔE detector was mounted on a movable external arm and used as the primary high energy proton detector, referred to as the PC detector. It was moved to cover the angular range of 12°–64° and subtended between 20 and 58 msr depending on its radial position. Two additional proton detectors of the smaller design, ≈ 12 msr, were also used, one at 120° in the reaction plane, and the other 25°–35° out of plain at the same θ angle as the PC detector. The dead layers in front of the external detectors placed a low energy cutoff of ≈ 40 MeV for protons and correspondingly higher values for the other H isotopes. The Si detectors were calibrated using standard alpha sources whereas the proton detectors were calibrated by detecting the *pp* scattering from a CH_2 target in pairs of detectors.

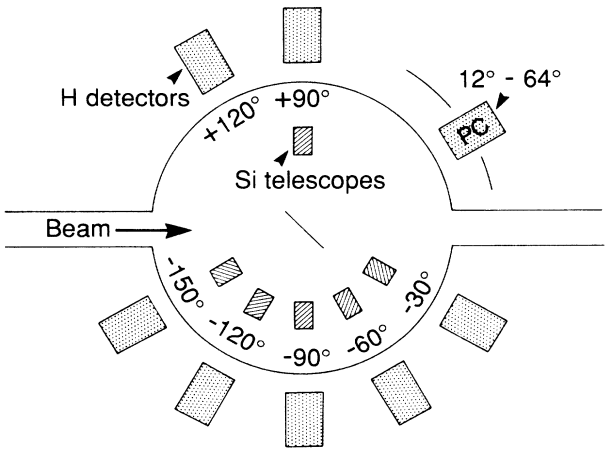

FIG. 1. Schematic experimental configuration.

A secondary emission monitor downstream of the chamber provided a measure of the beam current. However, the direct comparison of the inclusive ^{4}He production to known cross sections proved to be a more accurate measure of the absolute beam current. Therefore, the absolute normalizations were determined by comparing the inclusive ^{4}He production at 90° with previous results.[33]

B. Electronics and data acquisition

Standard NIM and CAMAC units were used to process the signals from the detectors. Both timing and linear signals from each detector were digitized and recorded. The timing gates were set wide enough so that events from a least three beam bursts (2.5 ns, 42 ns apart including the prompt burst) would be collected. The contribution of random coincidences for each pair of detectors was determined from the observed rate for that pair in the adjacent beam burst. True to random rates were always in excess of 10 to 1 and were as high as 50 to 1 for some detectors. The PC detector determined the start time for all events in which it was involved. When any two of the other detector systems registered events without a PC event, the start time was dependent on the specific detectors involved. Charge integrating analog-to-digital converters (ADC's) were used for all linear scintillator signals and peak sensing ADC's were used for the Si detectors. Logic signals identifying which detectors had fired were recorded in bit registers. In addition, scalers were used to monitor and record various parameters of the experiment.

The logic of the experiment was set to accept any coincidence, whether it involved the PC detector or not. In addition, singles events were recorded simultaneously for all detectors by prescaling their rates to prevent their dominance in the recorded data. This allowed a direct comparison between exclusive and inclusive spectra and was also an effective way to normalize the data. Pulser events were also collected simultaneously to monitor the detector responses. Off-line analysis of the pulser events indicated that no count rate corrections needed to be applied to the data. Due to the large difference in the electronic processing time between the fast scintillator detectors and the slow Si detectors, each event was initiated by a fast initial decision and confirmed by the slow Si logic. If the slow logic was not satisfied, the event was rejected and a fast clear pulse applied to the electronics. The fast clear requests were generally a small fraction and always less than 50% of the true events, and the procedure did not significantly add to the dead time of the experiment.

The computer acquisition system limited the data collection rate to under 100 events/s with live times of 70–90 %.

C. Data reduction

The off-line analysis of the data started with the selection of the time bins for each type of event so that gates could be set to select real events. In addition, the prompt and random beam bursts were identified and used to correct the coincident events for those events which occurred in the same beam burst but from different interactions. Identical initial analyses were performed on the prompt and random events and then subtracted to give the true coincidence events. Since the true to random event rates were in excess of 10 to 1, these corrections were generally small.

The particle identification of the fragments stopped in the Si telescopes was calculated by the algorithm described in Ref. 36. Similarly, the external detectors behind the Si telescopes used the same algorithm, but the energy signal from the Si telescope was used as the ΔE value. The ΔE scintillators in front of the external detectors were primarily used to cut down on background on a fast time scale by requiring a coincidence between them and the E detector. An arbitrary function of the Si E signal, to correct for the energy loss from the dead layer due to the intervening chamber wall, and the calibrated E scintillator energy value were used to identify the protons and determine their total energies. The response function of the external detectors was calculated by the procedure described in Ref. 34. To correct the coincidence rate for the change in the proton spectrum as a result of this response function, the coincident spectra were modified by a ratio of the corrected to uncorrected proton values energy bin by energy bin. This correction was generally less than 10%.

The singles spectra offered both a check on all of the experimental corrections and a method for absolutely normalizing the results. A comparison of the ^{4}He spectra from Ag, as measured by the $\pm 90°$ Si telescopes, with the previously reported values,[33,36] is given in Fig. 2. The slight differences in magnitude between the two data sets

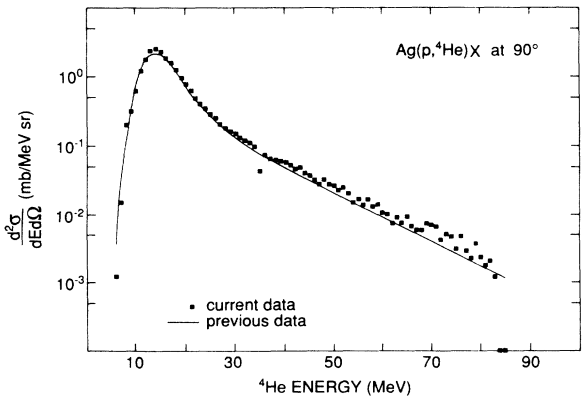

FIG. 2. Comparison of present inclusive ^{4}He spectra at 90° in the lab from a Ag target with fitted previous data.

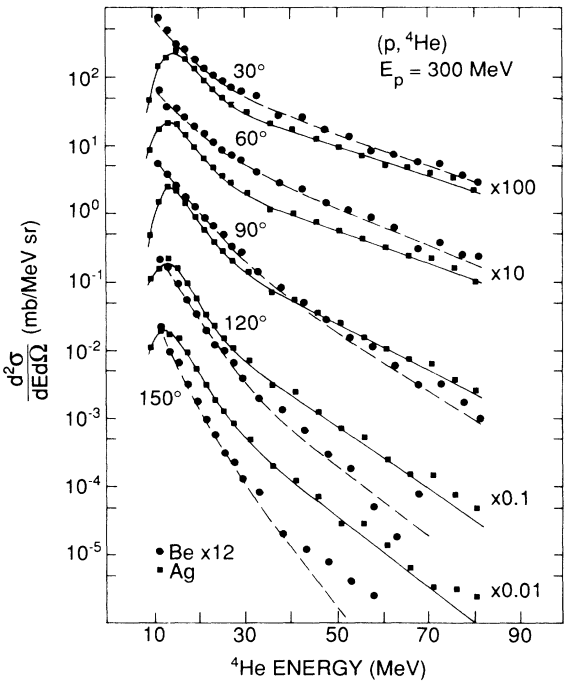

FIG. 3. Comparison of inclusive ^{4}He spectra from Be and Ag targets at various lab angles. The curves are parametrized fits to the data. Data from Be have been multiplied by 12.

can be explained by a displacement of the beam spot of 2–3 mm from the mechanical center of the chamber or an error in the claimed active area of one or more of the individual Si detectors. In either case, the calculated solid angles for the two Si telescopes would be in error and the weighted sum would be different from the $-90°$ data used for normalization. The slight shift in the peak energy is within the errors associated with target thickness corrections and energy binning of both these data and those reported previously. The low point at 35 MeV is due to the dead layers between the second and third Si detectors in the Si telescopes. The data end at 83 MeV in agreement with detector range calculations. Similar comparisons were made for the ^{4}He emission from Be and likewise were used to normalize the Be results. The statistical fluctuations of the data points reflect the propagation in quadrature of all statistical errors.

To facilitate the analysis of the data, it is convenient to have smooth fits of the individual particle spectra. The He spectra from Ag are complex in that there is a Coulomb barrier cutoff at low energies and a change in slope in the logarithmic decrease as a function of fragment energy at the higher energies. A two-component fit based on the parametrization described in Ref. 32 was applied. The He spectra from Be do not have the Coulomb cutoffs and a simpler standard smoothing procedure was used. Comparisons with the two-component fitting procedure gave similar results. Figures 3 and 4 illustrate these fits.

A series of energy cuts on the high energy protons detected in PC in coincidence with the He fragments were made to illustrate the variation in He emission as a

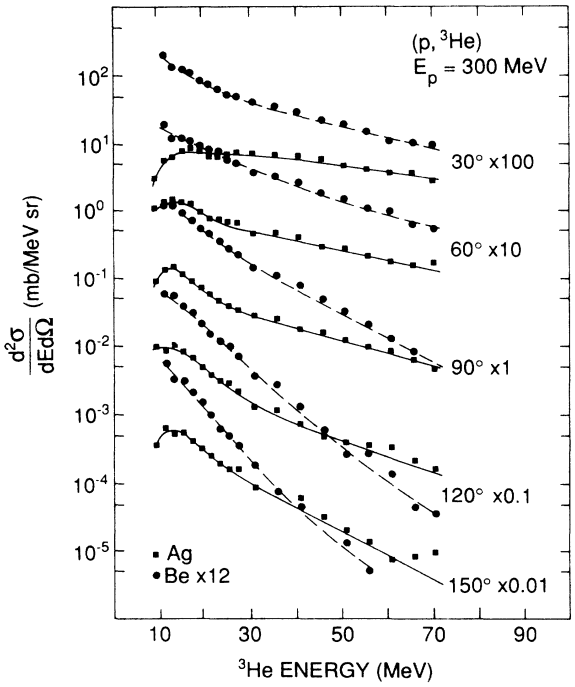

FIG. 4. Same as Fig. 3 except for ^{3}He emission.

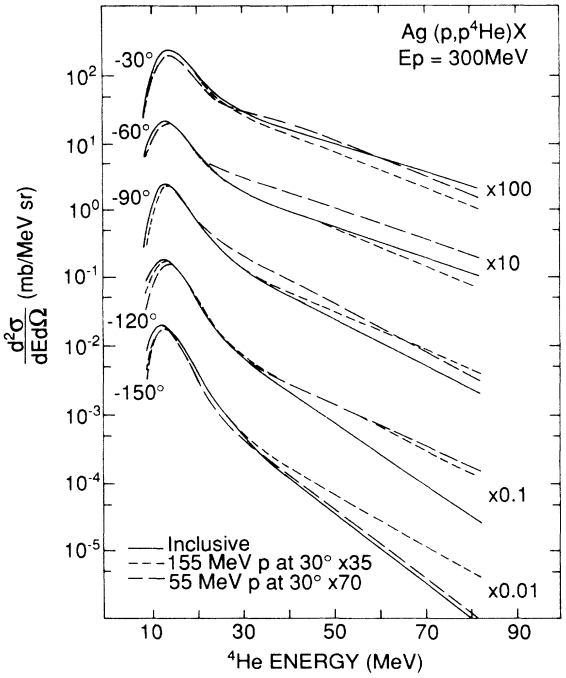

FIG. 5. Comparison of inclusive ^{4}He spectra and ^{4}He spectra in coincidence with 55 and 155 MeV protons emitted at 30° from a Ag target at various lab angles.

function of coincident proton energy. These cuts also permitted an estimation of the energy and momentum remaining in the system leading to the fragment emission. They were for 10 MeV bins centered on 55, 105, 155, 205, and 245 MeV protons. The binwidth was a compromise between minimum momentum widths and reasonable statistics. In the remainder of the paper coincident protons will be referred to by these energies and it is to be understood that in reality there is a 10 MeV binwidth involved.

III. ANALYSIS AND DISCUSSION

A. Particle spectra

The similarity of the inclusive He production from as diverse targets as Be and Ag has been noted previously[33] and is substantiated in this study. Figures 3 and 4 illustrate the comparison where the He emission from Be and Ag is directly compared with the Be data multiplied by the ratio of the Ag to Be masses, a factor of 12. The data have been binned in 2 and 5 MeV bins to decrease the statistical fluctuations and to make the figures more intelligible. The solid curves are fits to the data and were done on the initial 1 MeV binned data. The functional form and the parameters used for the fitting are discussed in detail in Refs. 32 and 33. The slope parameters obtained from the current fits are comparable to the previously reported values of 13.1 and 18.1 for ^{3}He emission and 8.5 and 14.6 for ^{4}He emission from Be and Ag, respectively.[33] Slight variations from these values for the numerous fits to the data, such as shown in Fig. 5, are not the subject of this study.

The spectra from Ag clearly show the effect of a Coulomb barrier from an emitting system with mass comparable to the target by their falloff at low energies. This low energy falloff is missing in the Be spectra, as expected. In making overall yield comparisons between these two targets, it should be noted that there is an increased forward peaking in the Be case reflecting a probable difference in the center-of-mass motion in the two target systems. Comparing the 90° emission values should minimize this difference on the spectra. At that angle, the ^{4}He cross sections from the two targets are virtually identical above the Ag Coulomb barrier region and the ^{3}He cross sections approach a common value at high fragment energies. The ^{3}He spectral shapes are much flatter from the Ag target than from the Be target reflecting the decreased relative importance of conventional evaporative processes on the low energy emission of ^{3}He from that target. In general, however, the similarities suggest that, on average, the processes leading to the emission of fragments, such as He, are comparable in both targets and that their probabilities are primarily related to target mass.

The He spectral shapes in coincidence with energetic protons are similar to the inclusive spectra. Figure 5 displays the fitted inclusive ^{4}He spectra and ^{4}He spectra in coincidence with 55 and 155 MeV protons emitted at 30° from Ag. Magnitudes have been adjusted between the sets of spectra to give agreement at $-90°$ and at $E_\alpha \approx 15$ MeV. A similar agreement is obtained when comparisons involving ^{3}He from Ag and ^{3}He and ^{4}He emission from Be targets are made. There does not seem to be a direct coupling between the He fragment emission and the coincident proton emission except for magnitude.

This is consistent with the notion of the formation of some intermediate emission source in a sequential two-step model.

On the other hand, the inclusive high energy proton spectra are noticeably different for the two targets, reflecting the greater influence of unaffected quasifree scattering in the light Be target. The differences are dramatic when viewed in coincidence with He emission in the energy range of 10–20 MeV. Figure 6 displays smoothed proton spectra measured at 17° where both inclusive and exclusive spectra are shown. In the Ag case, the inclusive and exclusive spectra are similar in shape and the magnitudes of the coincident spectra are comparable. This is not the case for the Be target where both the shape of the inclusive and exclusive spectra are different as are the individual exclusive spectra. The enhancement of the high energy protons in the coincidence cross section for the Be versus Ag target emphasizes the role the target mass plays in the emission process. In the Be case, the cross section is maximized when a minimum of energy is transferred to the target system and final-state interactions are minimal, whereas the opposite is the case for a heavy target such as Ag where final-state interactions seem to have a strong effect on the emitted proton and wash out any structure.

These differences become clearer when contour plots of the coincident data are viewed. Figures 7 and 8 display the ^{4}He emission from Be and Ag in coincidence with protons detected at 54°. The coincidence cross sections were arbitrarily fitted with seven contour levels at each angle. Thus, the levels from one angle cannot be directly related to those of an other without a knowledge of the magnitude of the cross sections at each angle. However, it does permit observation of the relative structures at each angle with maximum resolution. Quasifree scattering of ^{4}He is visible in the Be data where a peak in the

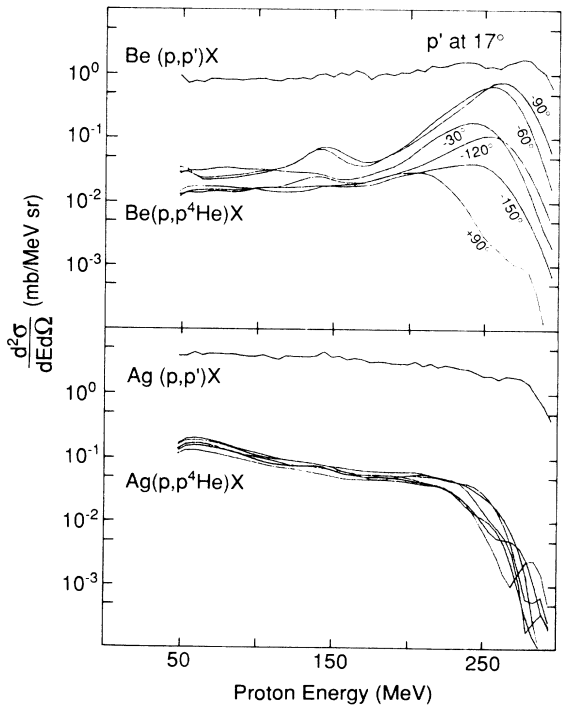

FIG. 6. Comparison of 17° inclusive proton spectra with proton spectra in coincidence with 10–20 MeV ^{4}He fragments emitted at various lab angles from Be and Ag targets.

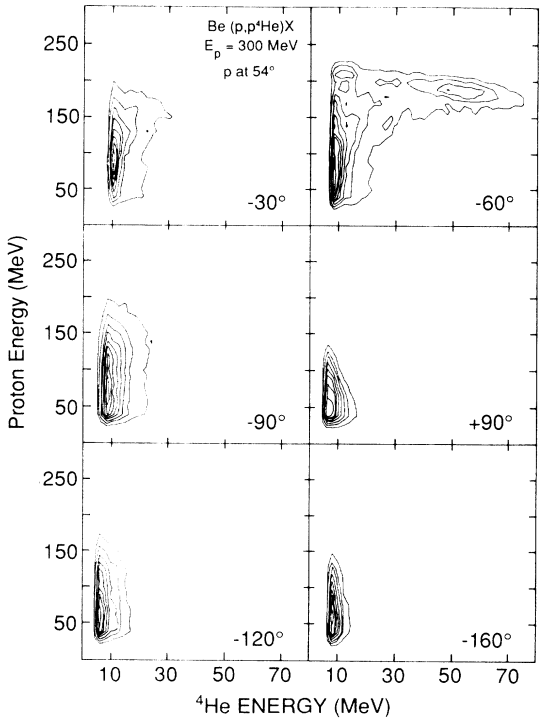

FIG. 7. Contour plots of ^{4}He emission at various lab angles in coincidence with protons emitted at 54° from a Be target.

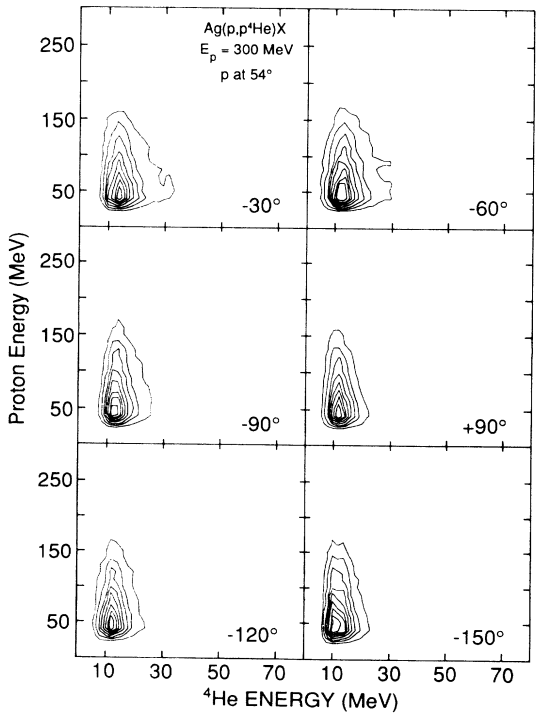

FIG. 8. Same as Fig. 7 except for a Ag target.

distribution occurs for ^{4}He emission at $-60°$ and ≈ 50 MeV. There is another smaller peak for 10 MeV ^{4}He and 210 MeV protons in the same frame due to the target residue left behind in the quasifree interaction. The enhancement of the high energy protons in coincidence with ^{4}He emission from Be is a result of the increased probability of knocking out or forming ^{4}He in such direct interactions. In fact, the peak in the coincident proton spectra from Be at 140 MeV for $-60°$ and $-90°$ ^{4}He emission, seen in Fig. 6, is at approximately the predicted *NN* quasifree scattering values if one of the nucleons were to lead to ^{4}He emission. This can be seen in the details of the contour plots not visible in these figures. These features are not observed in the Ag case and indicate that the effects of quasifree scattering are washed out by final-state interactions in such a complex target. However, except for these specific cases of direct interaction components in the emission of fragments from Be, the majority of the cross section is very similar between the two target systems leading to the similar results mentioned above.

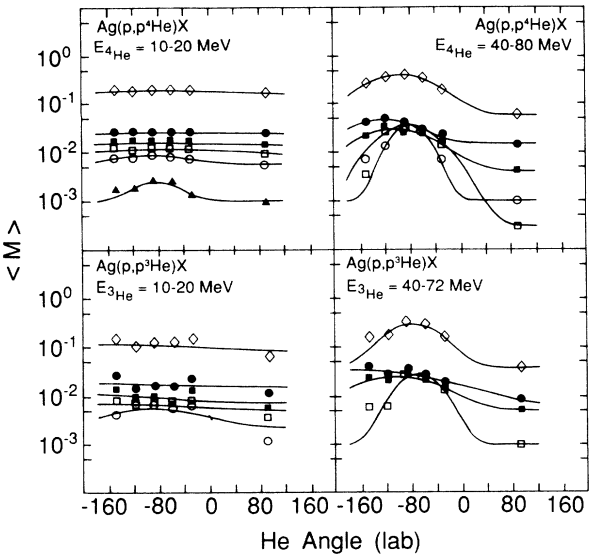

FIG. 10. Same as Fig. 9 except for a Ag target.

B. Proton differential mean multiplicities associated with He emission

In order to show how these cross sections vary as a function of emission angle and coincident proton energy, the ratio of the coincident cross section to the corresponding inclusive cross section has been calculated. This double-differential mean multiplicity is defined by[34]

$$\frac{d^2\langle m\rangle}{dE_f d\Omega_f} = \frac{d^4\sigma(E_q,\theta_q,\varphi_q;E_f,\theta_f,\varphi_f)/dE_q d\Omega_q dE_f d\Omega_f}{d^2\sigma(E_q,\theta_q,\varphi_q)/dE_q d\Omega_q},$$

where the coincident fragment is q. Figures 9 and 10 display typical examples of the results of integrating $d^2\langle m\rangle/dE_f d\Omega_f$ over limited ranges in part of its variables. The symbol $\langle M\rangle$ is used to indicate such partial integrations. The figures are for He associated proton emission at 30° with respect to the beam, for a selection of fragment and proton energies as a function of the fragment emission angle. The curves are drawn to guide the eye and were generated by fitting the angular distribution with a Gaussian superimposed on a constant isotropic background. While these differential mean multiplicities are nearly isotropic for low energy ^{3}He and ^{4}He from Ag, all other cases show a maximum in the vicinity of $-80°$ to $-120°$. Only when the highest energy coincident protons are involved is there any deviation from isotropy for the low energy He emission from Ag. There is also a tendency for there to be more structure when either the He or the proton has higher energy. If the low energy ^{4}He emission from Ag is dominated by evaporation from a pseudocompound system, as has been argued,[32,36–38] its relatively flat differential mean multiplicity could be understood. Similarly, such arguments would suggest that for all the other cases, a more direct mechanism may be dominating. But this argument may be too simplistic since the evaporative component of ^{3}He is believed to be small even from Ag (Ref. 32) and yet the low energy ^{3}He fragments show the same behavior as ^{4}He.

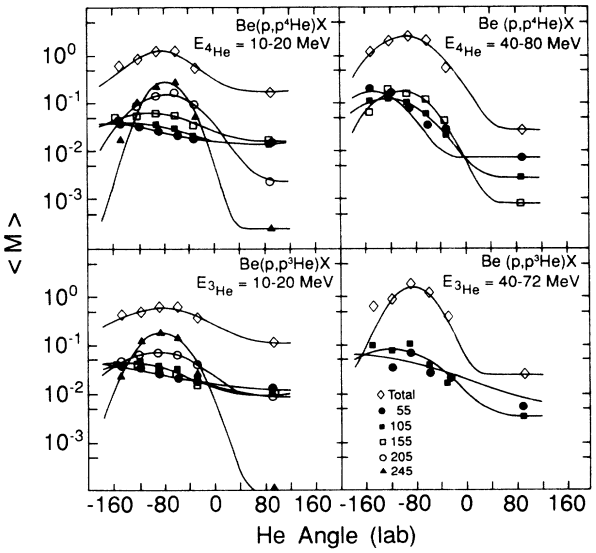

FIG. 9. Plots of the proton differential mean multiplicities integrated over the ranges indicated for He emission from a Be target as a function of He emission angle and coincident proton energy. Protons were emitted at 30°. The smooth curves are fits to a Gaussian plus a constant. The symbols indicate the different coincident proton energy cuts.

The agreement between the location of the maximum in the differential mean multiplicities and the QTBS (quasi-two-body scaling) angle was used as an argument for direct scattering being a dominant mechanism for the interaction in an analysis of the $(p,2p)$ and (p,pd) reactions on Be with 300 MeV protons.[34,35] Figure 11 compares the predicted QTBS angles for 30° proton emission with the angles of the Gaussian maxima obtained from Figs. 9 and 10, and similar figures for other coincident proton angles, for high energy He emission as a function of coincident proton energy and angle. The other coincident proton angles will generate similar QTBS curves

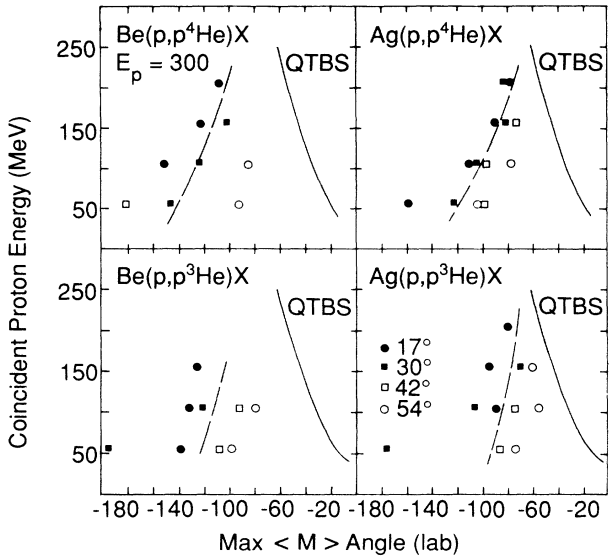

FIG. 11. Plots of the angle of the maximum in the differential mean multiplicities for Be and Ag (p,pHe) reactions as a function of coincident proton energy and angle. The ^{4}He energy is integrated over 40–80 MeV and the ^{3}He energy from 40–72 MeV. The solid curve is the predicted QTBS angle, the dashed curve is to guide the eye for the proton energy dependence.

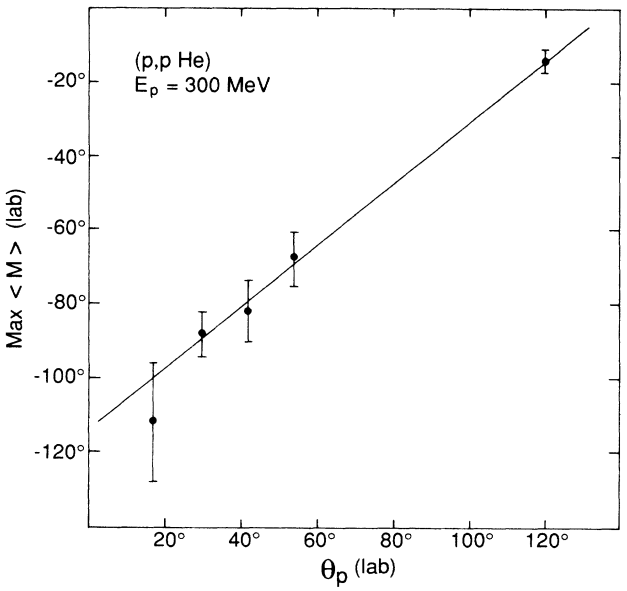

FIG. 13. Angular dependence of the He angle of maximum energy integrated differential mean multiplicities as a function of the coincident proton angle. Data from low energy He emission from Ag are not included.

displaced by no more than 20°. The dashed line is drawn to guide the eye in determining the trend of the measured Gaussian peaks with coincident proton energy. Although there is significant scatter in the values as a function of coincident proton angle, the maximum in the angular distributions is significantly shifted to larger negative angles in a trend opposite to that expected for QTBS dominated emission. This suggests that except for the high energy cases, QTBS emission is not dominant in this data. This is not surprising since the momenta involved are not in the region which strongly drives the QTBS mechanism.

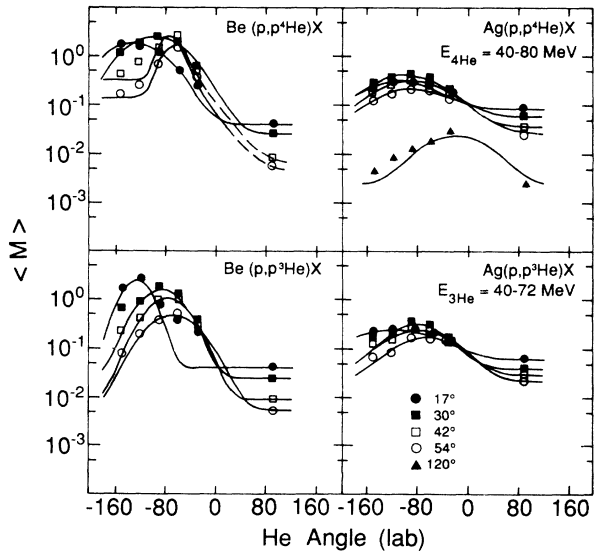

FIG. 12. Plots of energy integrated differential mean multiplicities from Be and Ag as a function of He emission angle and coincident proton angle. Data from low energy He emission from Ag are not included. Symbols are the same as Fig. 11 with the addition of solid triangles for 120°.

In additional to the shift in the locations of maximum differential mean multiplicities as a function of coincident proton energy, there is a general shift as a function of proton angle. This shift is seen in Fig. 12 where the proton differential mean multiplicities for He emission from Be, integrated over all measured He energies, and high energy He emission from Ag are plotted for various coincident proton angles, integrated over all measured proton energies. These curves have been fitted with a Gaussian plus constant form. The He angles corresponding to the maximum values in these fits were averaged for each proton angle and these averages are displayed in Fig. 13. Since the low energy He isotopes from Ag were essentially constant as a function of coincident proton energies and angles, they were not included in determining these mean angles. The solid line is a linear fit to the points. These data show that the most probable angle between the He fragment and a coincident energetic proton is nearly constant over a range of proton angles from 17° to 120°, with a value of about 120°, and is consistent with a two-body breakup mechanism. The angular dependence suggests an average opening angle of 120°–130°. The gradual shift of the maximum seen in Fig. 11 from near the QTBS angle to larger negative angle emission, as a function of decreasing observed proton energy, may reflect the changing dominance of two different processes in this data.

C. Moving source analysis

A rapidity analysis of the data is most instructive. Sets of points in the $(Y,p_\perp/mc)$ plane at which the invariant

cross sections $(1/p)(d^2\sigma/dE\,d\Omega)$ are identical can be extracted from the smooth fits of the He data. The fragment's rapidity, $y=\tanh^{-1}\beta_{\parallel}$, and its transverse momentum, $p_{\perp}/mc$, are essentially its parallel and perpendicular velocities $\beta_{\parallel}$ and $\beta_{\perp}$, respectively, since the velocities are low ($\beta \leq 0.2$). These sets of points can be used in a rapidity analysis similar to that described in Ref. 32. Examples of the invariant cross section contours of the ^{4}He emission from Be and Ag targets in this plane are given in Figs. 14 and 15. The circular contours are least-squares fits to the data points with their centers displayed as a series of dots. The contours are logarithmic with three levels to a decade. No fits could be made for the case of ^{4}He emission from Be in coincidence with 205 MeV protons at 54°. The small + symbol represents the velocity that a compound nucleus would have if momentum were conserved between the incident proton, the target, and the observed exit proton. Plots of ^{3}He emission show the same general trends but since the ^{3}He spectra are flatter than those for ^{4}He, there are fewer contours and therefore the ^{3}He results have not been displayed.

The similarity between the plots for inclusive ^{4}He emission from Be and Ag and the good agreement with the circular fits is remarkable and further illustrates the similarity for fragment emission from these two diverse target nuclei when viewed in total. The centroids show the approximate linear relationship between source velocity and fragment velocity noted before.[32] Similar good agreement with circular fits is observed if He emission is selected on low energy coincident proton emission. However, as the energy of the coincident proton is raised, the fits start to deteriorate, as illustrated in the case for a coincident 155 MeV proton at a 30° trigger. The deviation is seen by an enhancement in ^{4}He emission at $\approx -60°$ and a decrease at adjacent angles suggesting a change from circular to elliptical shapes as a function of ^{4}He energy. By selecting a specific coincident proton, an average source has been selected which reflects the momentum constraints of the measurement and the centroids are displayed in accord with the conservation of transverse momentum. The results for coincident 245 MeV protons at 17° is a special case. Although the deterioration of the fits is evident for both targets, the centers of the contours for the Be target data coincide with the predicted displacement for a resultant "compound nucleus." This is not so for the Ag target. This Be data represents the only clear case of agreement with the notion of a total target nucleus forming an emitting source. Finally, the effect of the quasifree scattering from ^{4}He seen in the coincident contour plots mentioned above (Fig. 7) is effecting the invariant cross-section distributions seen in the case for 205 MeV protons detected at 54°. The ovals simply connect the points of constant invariant cross section for the Be case. For the Ag case, there seems to be an enhanced deviation from circular symmetry and may suggest some quasifree scattering not noticeable in the more crude coincident contour plots.

The agreement of circular fits with constant invariant cross section has been a strong argument in favor of describing fragment production as isotropic emission from an equilibrated source. These results both support such interpretations and draw attention to the danger of interpreting highly average values in such a detailed manner. The inclusive results are examples of very good agreement with the notion of isotropic emission from a moving source but they are themselves an average of other contours which are sometimes circular and sometimes not as seen in the coincident displays. Furthermore,

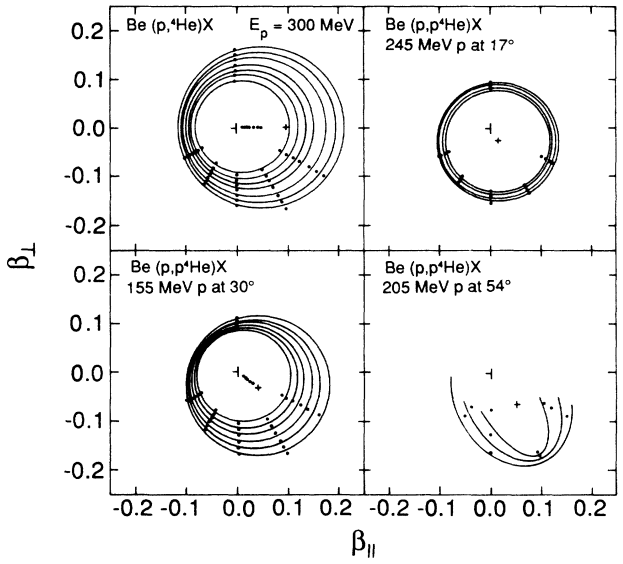

FIG. 14. Perpendicular versus parallel velocity plots of invariant cross-section contours for ^{4}He emission from a Be target for various inclusive and exclusive cases. Circular plots are logarithmic contour levels fitted to the data. Small dots in the center are the centers of the circular fits. The small plus symbols are the nominal compound nucleus velocities. No fits could be made for the 205 MeV proton at 54° case and the ovals are drawn to connect the points of constant cross section.

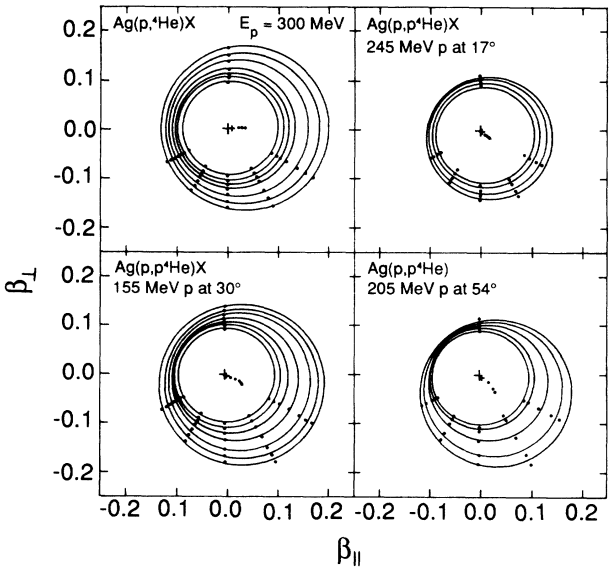

FIG. 15. Same as Fig. 14 except for a Ag target.

selecting on specific proton energies does select certain average sources but does not uniquely identify a source. Setting aside these concerns for the moment, the fact that the source velocities, as measured by the centroids, are not those expected for pseudocompound nuclei, shows that such sources must be a small subset of the target nucleus. In the Be case where the source velocities are smaller than that for the predicted compound nucleus, much of the momentum and corresponding energy must have been carried of by another particle or particles. For the Ag case where the source velocities are greater than the compound nucleus value, only a smaller part of the nucleus could have been involved.

It is also important to note that the deviations from isotropic emission occur for the cases when the coincident proton energy is the greatest or when there is a large transverse momentum component. The energy dependence is the opposite of that expected if the assumption is made that the remainder of the unmeasured energy and momentum is transferred to the emitting source. Under such an assumption, the most likely isotropic emitting sources would be those with lowest source excitation energy corresponding to the highest coincident proton energies. Only if a major share of the energy and momentum is removed by particles not involved with the source could the observed dependence be explained. A clearer measure of the isotropic emission dependence on the energy or momentum transfer seems to be given by the transverse momentum component as calculated from the observed coincident proton. In general, deviations from circular symmetry occur when the transverse momentum exceeds 300 MeV/c, or in other words, when the transferred momentum exceeds the normal Fermi momentum within the nucleus.

Closer scrutiny of the source and radial velocities reveal interesting trends, as measured by the centroids of the circular contours fitted to the data and the corresponding contour radii. Figures 16 and 17 display the source velocity dependence on the fragment radial velocity and the source parallel and perpendicular velocities as a function of coincident proton energy and angle for a few typical cases. In general, the source velocity dependence on the radial velocity (Fig. 16) has approximately the same slope for all coincident proton energies but the data are shifted to higher β_s values as the energy of the coincident proton increases. This shift with proton ener-

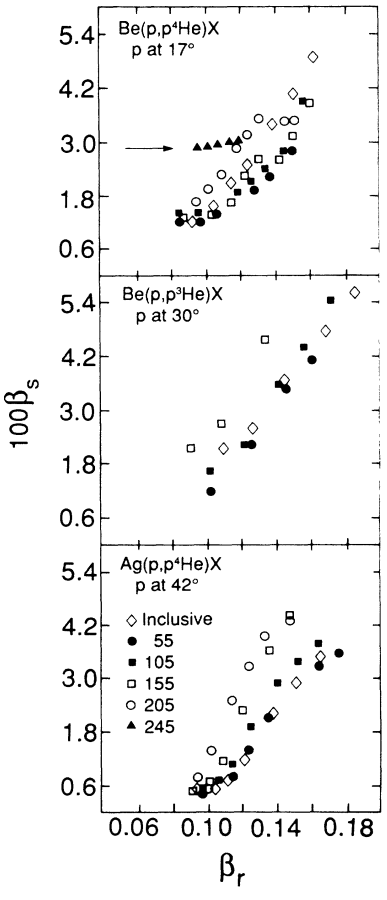

FIG. 16. Plots of source velocity β_s vs He radial velocity β_r as a function of coincident proton energy for a few typical cases as well as inclusive He emission. The arrow draws attentions to the special case where a "compound nucleus" was formed as described in the text.

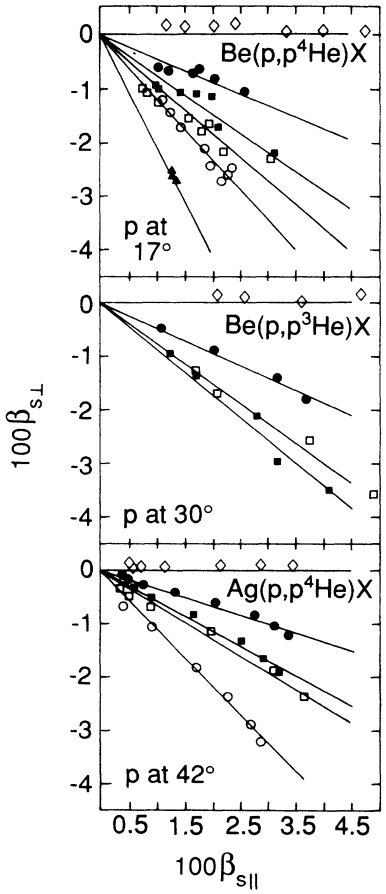

FIG. 17. Plots of perpendicular versus parallel source velocities for He emission as a function of coincident proton energy for the same cases presented in Fig. 16. Lines are fits to the data as explained in the text.

gy may be related to an increase in the fraction of the imparted momentum to the rest of the system remaining in the source as that momentum decreases. The source parallel and perpendicular velocities (Fig. 17) also exhibit a linear relationship. However, these slopes increase with increasing coincident proton energy, and therefore transferred perpendicular momentum, in a understandable way. These slopes are just $\tan\vartheta_s$, where ϑ_s is the source emission angle. The lines in Fig. 17 are the result of a linear fit to the data with the origin forced to be zero except for the inclusive data. The deviation from the drawn $\beta_{s\perp}=0$ line for the inclusive data points indicates the uncertainty of this analysis.

The case for ^{4}He emission from Be in coincidence with 245 MeV protons at 17° in Figs. 16 and 17 is an anomaly which results from the formation of a resultant "compound nucleus" source with the remaining energy and momentum in the system. This source has a definite momentum and velocity, as seen in Fig. 16. The arrows in the figures draw attention to this special case where the source velocity is $\beta\approx0.030$. A detailed look at the case for 205 MeV protons in the same figure suggests that the source velocity there reaches a maximum at about $\beta\approx0.033$ and then remains constant, but that may simply be experimental fluctuations.

The average dependence of the source velocity on the fragment radial velocity for both He isotopes from both targets is shown in Fig. 18. It is striking that the main feature is the agreement in slope for all cases over most of the range that has been measured. The slope values of 0.47 and 0.51 for the Be and Ag cases, respectively, are probably within experimental error. The line through the Be results was a fit to both the ^{3}He and ^{4}He data. The ^{4}He data from Ag were fitted with two lines, one excluding the bottom two points and the other using the bottom three points and the origin giving a slope $\frac{1}{10}$ that of the rest of the data. The clear break in the slope is in the

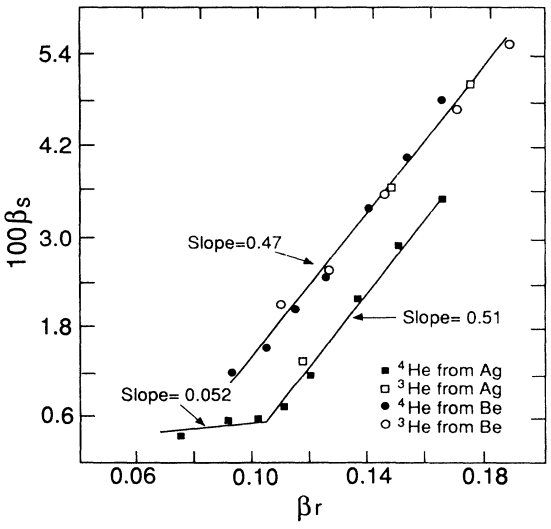

FIG. 18. The source velocity β_s dependence as a function of the He radial velocity β_r for inclusive He emission from Be and Ag targets.

15–18 MeV ^{4}He energy range emphasizing a dramatic change in the emitting source, probably from a pseudocompound nucleus to a small subset of the target. Furthermore, it should be noted that the low energy ^{3}He values from Ag are on the corresponding ^{4}He curve but shift to the Be curve at higher energies. This agrees with the previously mentioned similarities between the low energy He isotope multiplicity dependencies. These Ag ^{3}He values were not used in determining the fits. Here the shift in β_s for a given β_r between Be and Ag is more likely a result of different average source masses than the imparted momentum mentioned above. Although it is not possible to be precise, with some reasonable assumptions such as forming similar excitation energy distributions as a function of momentum transfer for the two systems, the difference between the two curves of less than a factor of 2 in β_s implies a difference in average source mass of less than a factor of 2.

The dependence of the source emission angle, as seen in Fig. 17, is summarized in Fig. 19, where the He source angle from the circular contour fits is plotted against the corresponding coincident proton energy for proton emission angles from 17° to 54°. The nucleon-nucleon quasifree angles are shown as curves for comparison. The correlation with the quasifree angle for the ^{4}He source angle from Be is remarkable and the agreement is within experimental scatter for the ^{3}He sources. The ^{4}He source angles from Ag have the same general shape as the quasifree dependence but are displaced to smaller angles by about 10°. One is drawn to the conclusion that an initial nucleon-nucleon collision must play a dominant role in defining the emitting source's angle, ϑ_s, in contrast with the lack of correlation between the He fragment emitted by the source and the proton as mentioned earlier. Subsequent final-state interactions probably wash out the angular dependence for the emerging proton, since there is no strong quasifree angular dependence on its emission, especially in the Ag target case.

Both this general agreement with isotropic emission from a moving source and the lack of correlation of fragment emission with the QTBS angle is an argument against a direct coalescence mechanism[39,40] for the production of fragments. A coalescence model assumes the generation of a fragment from nucleons of comparable momentum resulting from a series of nucleon-nucleon collisions. The fragment emission angle would then be correlated with the initial nucleon scattering angle. The observation of isotropic emission is not consistent with such a model. However, the strong source angle dependence with the scattering angle of the unobserved nucleon initiator of the source suggests that the source could be explained by its formation through such a mechanism.

The lack of any significant analyzing power in the emission of the He isotopes from a Ag target bombarded by intermediate energy polarized protons[41] was seen as a constraint on the direct interaction models of fragment production. The dominance of emission from some intermediate source suggested by these results is consistent with that earlier study. Unfortunately, that earlier study was a measurement of the inclusive He emission where

specific kinematic regions were not selected. It would be interesting to now select those regions where the rapidity analysis has suggested that deviations from isotropic emission from an emitting source occur to see if there is a direct scattering component present or if an intermediate source is involved even there.

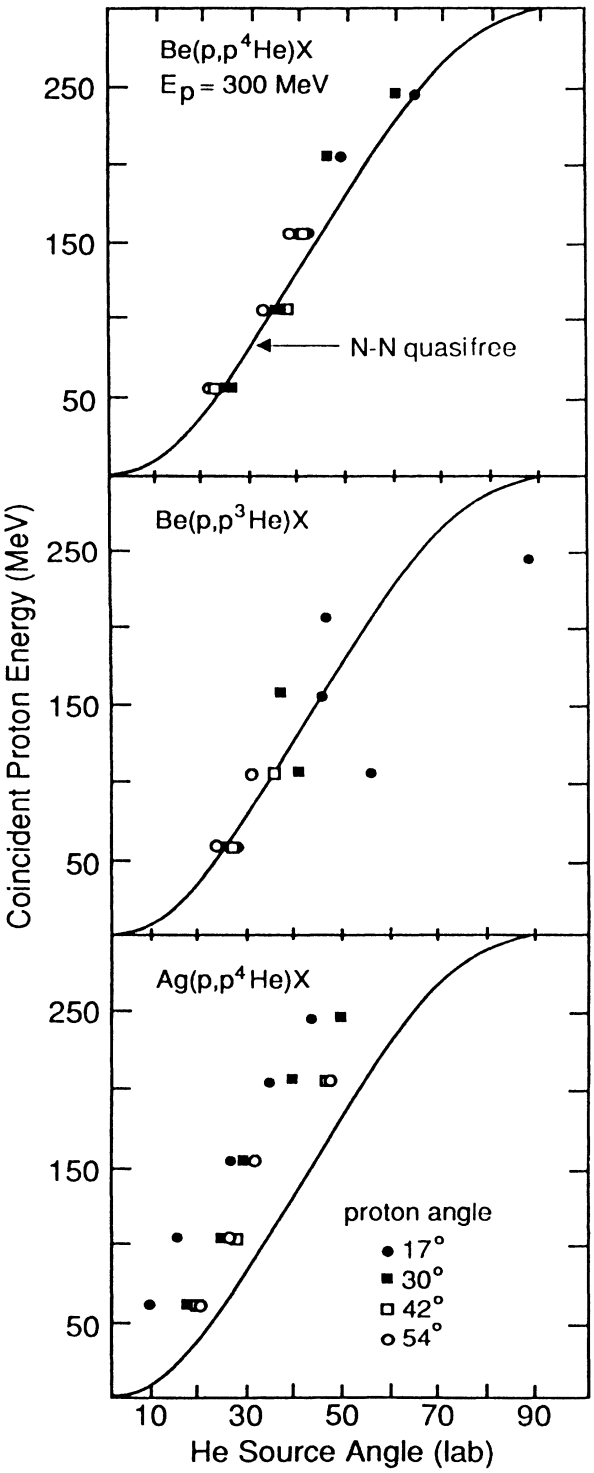

FIG. 19. Plots of the He source angles versus the coincident proton energies for various proton emission angles from Be and Ag targets. The solid lines are the nucleon-nucleon quasifree scattering angles.

D. Kinematic constraints

Although deviations from circular symmetry exist in the invariant cross-section analysis and are an indication that more direct processes may be important in the emission of fragments, the surprising general feature is the degree of agreement with such symmetry for the majority of the kinematic range covered by these measurements, even for the simple Be system. These average results may be understood in terms of the energy and momentum balances. For fragment emission to occur, a considerable amount of momentum must be conserved in the opposite direction. Although multiple scattering and final-state interactions can contrive to satisfy that requirement in most cases, the simplest means is for an excited source to deexcite by an effective binary breakup. This is supported by the observations of the structure in the mean multiplicities mentioned above and that the inferred source masses from the above rapidity analysis are generally small. This small size for emitting sources has been noted previously[32,41,42] and agrees with the predictions of factorizability for a sequential process.[43]

Additional experimental information concerning such a mechanism can be obtained by investigating fragment-fragment coincidences. The probability of observing a 6–12 MeV H or 8–82 MeV ^{4}He particle in coincidence with a ^{4}He fragment at 90° is displayed in Fig. 20 for both Be and Ag targets. The lines are drawn to connect the points and are not a fit to the data. Although there are differences between the two targets, the main feature is the dominance of emission in opposite hemispheres. The observed structures in these figures are intriguing and suggest that specific reactions involving particle unstable

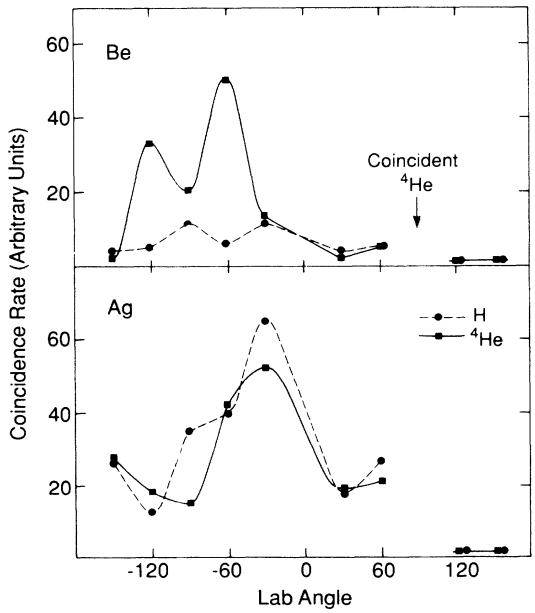

FIG. 20. Display of the relative emission probability for 6–12 MeV H and 8–82 MeV ^{4}He fragments in coincidence with ^{4}He emission at 90° from Be and Ag targets as a function of laboratory angle.

states of relatively light systems may play an important role, but it is beyond the scope of this paper to analyze that information in detail. Rather, simply the importance of directly balancing the momentum in the deexcitation of a source is demonstrated by these data, realizing that only two of the emitted particles have been observed. The lack of isotropic emission argues against a conventional evaporative mechanism from a relatively large emitting source, even for the Ag case.

If a mechanism is assumed where a binary split is the primary mode of deexcitation of a source formed by some initial interaction, simple kinematic calculations can be made using the measured proton and fragment energies and angles, and the source velocities inferred from the rapidity analysis. Although such calculations cannot be used to prove the validity of a model, they are useful in placing limits on the mechanism for reasonable initial assumptions. Figure 21 is a schematic representation of such a mechanism. Particles X and N' have not been observed in these measurements.

The range of possible source masses for ^{4}He emission from a Be target is 5–8, assuming at least one target nucleon in addition to the scattered nucleon is involved in removing the excess momentum and energy mentioned above. Conservation of momentum can be used to predict the remaining momentum carried off by the residual unmeasured system. There results a strong angular correlation of the unmeasured momentum components in the interaction to the nucleon-nucleon quasifree angle of an undetected nucleon partner to the detected proton. Similar results are obtained when a Ag target is used and interestingly, similar small source masses are required to balance momentum.

Changing the coincident proton angle, and therefore moving it out of the quasifree range, does not dramatically change the emission angles for the sources as determined from the rapidity analysis of the data, but does change the other unobserved components of the interaction to conserve momentum. Conversely, changing the proton energy does change the source angle determined in the data analysis such that it agrees with the shift in the predicted quasifree angle of the undetected nucleon. Such behavior suggests that the observed proton may have been significantly affected by final-state interactions after the initial interaction which formed the source. The source, on the other hand, seems impervious to such effects and reflects a strong initial nucleon-nucleon quasifree angle dependence.

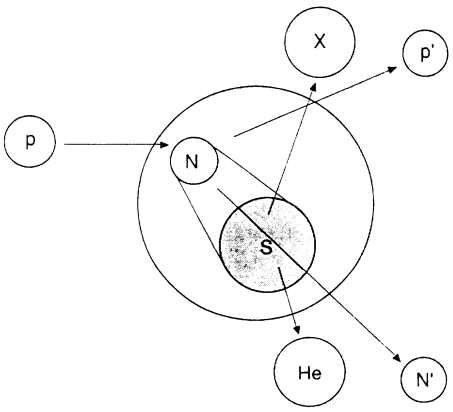

FIG. 21. Schematic proton-induced fragmentation reaction. N Represents a nucleon, X an unknown partner to the emitted He fragment, and S the fragment emitting source.

An attempt was made to check whether this model for fragment emission could be substantiated by a microscopic calculation of the initial proton interaction with the target nuclei. The Quasiparticle Dynamics code developed by Boal *et al.*[44,45] was used. Although it has had considerable success in reproducing the results of many heavy-ion studies, we found that it was unable to predict the production of composite particles from Ag by large factors even though it did represent proton emission remarkably well. The addition of an evaporative calculation would indeed lead to some fragment emission from the excited targetlike residues, but these would be at lower fragment energies. The code's inability to reproduce the high energy fragment production, where the contribution from conventional evaporation will be minimal, suggested that preemission cluster formation may be important in proton and light-ion reactions, a feature which the code did not include.

IV. SUMMARY AND CONCLUSIONS

The similarity of inclusive light fragment production, as monitored by He emission, between two diverse targets such as Be and Ag has been illustrated. Their ^{4}He emission singles spectra are of the same general shape and differ mainly in magnitude by the ratio of the target masses and in angular dependence due to kinematic effects resulting from the different target masses. The ^{3}He spectra are somewhat different with the emission from Be having the same slope and magnitude as ^{4}He spectra whereas the ^{3}He spectra from Ag are flatter than those for ^{4}He at the lower fragment energies. A rapidity analysis of these inclusive spectra generates good agreement with circular contours of constant invariant cross section and gives a direct relationship between the He radial velocity and a source's velocity. When an exclusive channel is selected, by observing a coincident proton, the same general similarity is still present. Further analysis of the inclusive data using the average source characteristics, inferred from the circular contours, imply a small emitting source for most cases for both targets. In addition, the angular structure in the differential mean multiplicities is similar for both targets although features for the Ag target are understandably not as sharp as those for the Be target. Only when the coincident proton energy spectra are studied is there a significant difference in the qualitative features of the two systems. The larger mass of the Ag target seems to have a significant effect on the final-state interactions involved in the proton's emission. However, this effect does not seem to be as important in the emission of fragments and again suggests that the processes involved in fragment emission are similar in the two extreme cases.

Although not investigated under the exact same condi-

tions, the general dependence on the QTBS angle observed for the $(p,2p)$ and (p,pd) (Refs. 32 and 34) reactions on Be is not seen in the more complex $(p,p\text{He})$ reactions, even for Be targets. Only the highest coincident proton energies show such a correlation for He emission. As the proton energy decreases to low values, the most probable laboratory angle for He emission approaches $-130°$. Recognizing that the lower energy protons may not be directly related to the initial interaction, or at least strongly influenced by final-state interactions, this change is reasonable and does not necessarily negate a model where primarily direct interactions dominate in the initial step of fragment emission.

The rapidity analysis of both the inclusive and exclusive measurements has shown how strongly averaged the data become in such an analysis. Care must be exercised in using these results in describing specific reaction channels even if they are model independent. Nevertheless, the dominant feature of this data is how well such an analysis does agree with concepts of statistical emission from a moving source, that is, isotropic emission in the source's frame. The main difference between the two targets is the larger source velocity for a given fragment velocity in the Be interactions. However, in the extremes the emission is not isotropic. Although the effects are not as pronounced for Ag as for Be, significant deviations appear when the target system is required to absorb momentum in excess of 300 MeV/c.

Noting these features of fragment emission and that a considerable amount of momentum must be conserved for a fragment to be emitted, a reasonable model of the process can be made by assuming that fragment emission is primarily the result of an effective binary breakup of an excited source slightly larger than the fragment. The fact that the emission probability for coincident particles is dominantly in the opposite hemisphere is supportive of such an assumption. The source is produced in some initial step which may be dominated by its quasifree interaction with some nucleon or nucleons which remove the excess momentum and energy. The emission angles inferred from the data for the sources are nearly equal to those of the recoiling partner in nucleon-nucleon quasifree scattering of the observed energy. The emission angle of the coincident proton, on the other hand, is not so constrained suggesting the importance of final-state interactions in its emission. The formation of this continuum of sources with varying excitations is consistent with the speculation of Remington *et al.*[25] of a small, hot source evolving into a larger, cooler source as a means to explain their heavy-ion results.

In general, the present results suggest that for proton-induced reactions, light fragment production may be dominated by relatively simple processes producing a distribution of small, excited sources which deexcite primarily by a binary breakup before forming relatively large equilibrated systems. However, some of the less excited sources may evolve into a large equilibrated system and then deexcite by the conventional evaporation process. Such a model can explain the relative insensitivity of fragment production to target mass and the continuum of fragment energies in a natural way and is a considerably different picture of fragment emission than normally presented. The inability of observing any significant direct component to fragment emission, such as QTBS dependent emission or analyzing powers, argues for such an intermediate step. Such a description would place constraints on the interpretations of coincidence particle emission presently used to study thermal properties of nuclei unless the system has been shown to be a relatively large equilibrated source by alternate means.

ACKNOWLEDGMENTS

The authors wish to thank N. Bohna for her assistance in processing the data through the Simon Fraser University Computing Center. A special vote of thanks is given to R. Abegg for his help in improving the beam tune and quality needed for the experiment. The help of the TRIUMF beam lines group in fabricating the scattering chamber is acknowledged as well as the effort of the operations staff in obtaining the proton beams used in this experiment. This work was supported by the Natural Sciences and Engineering Research Council of Canada and by the U.S. Department of Energy, Nuclear Physics Division, under Contract W-31-109-ENG-38.

*Present address: Los Alamos National Laboratory, Los Alamos, NM 87545.

[1]D. H. Boal, Adv. Nucl. Phys. **15**, 85 (1984).
[2]W. G. Lynch, Annu. Rev. Nucl. Part. Sci. **37**, 493 (1987).
[3]W. G. Lynch, Nucl. Phys. **A471**, 309c (1987).
[4]W. A. Friedman, Nucl. Phys. **A471**, 327c (1987).
[5]C. J. Pethick and D. G. Ravenhall, Nucl. Phys. **A471**, 19c (1987).
[6]D. H. E. Gross and H. Massmann, Nucl. Phys. **A471**, 339c (1987).
[7]J. Randrup and S. E. Koonin, Nucl. Phys. **A471**, 355c (1987).
[8]C. Gregoire, D. Jacquet, M. Pi, B. Remaud, F. Sebille, E. Suraud, P. Schuck, and L. Vinet, Nucl. Phys. **A471**, 399c (1987).
[9]S. Das Gupta, Nucl. Phys. **A471**, 417c (1987).
[10]D. H. Boal, Phys. Rev. C **28**, 2568 (1983); **29**, 967 (1984); **30**, 749 (1984).
[11]G. Sauer, H. Chandra, and U. Mosel, Nucl. Phys. **A264**, 221 (1976).
[12]H. R. Jaqaman, A. Z. Mekjian, and L. Zamick, Phys. Rev. C **27**, 2782 (1983); **29**, 2067 (1984).
[13]M. W. Curtin, H. Toki, and D. K. Scott, Phys. Lett. B **123**, 289 (1983).
[14]D. H. Boal, Annu. Rev. Nucl. Part. Sci. **37**, 1 (1987).
[15]G. E. Beauvais, D. H. Boal, and J. Glosli, Nucl. Phys. **A471**, 427c (1987).
[16]D. Scott, Nucl. Phys. **A354**, 375c (1981).
[17]D. H. Boal and J. C. Shillcock, Phys. Rev. C **33**, 549 (1986).
[18]J. Pochodzalla *et al.*, Phys. Rev. Lett. **55**, 177 (1985); Phys. Lett. **161B**, 275 (1985).
[19]H. M. Xu *et al.*, Phys. Lett. B **182**, 155 (1986).
[20]C. B. Chitwood, C. K. Gelbke, J. Pochodzalla, Z. Chen, D. J.

Fields, W. G. Lynch, R. Morse, M. B. Tsang, D. H. Boal, and J. C. Shillcock, Phys. Lett. B **172**, 27 (1986).
[21]J. Pochodazalla, Nucl. Phys. **A471**, 289c (1987).
[22]D. J. Morrissey, W. Benenson, E. Kashy, B. Sherrill, A. D. Panagiotou, R. A. Blue, R. M. Ronningen, J. van der Plicht, and H. Utsunomiya, Phys. Lett. **148B**, 423 (1984); Phys. Rev. C **32**, 877 (1985); **34**, 761 (1986).
[23]W. G. Lynch, L. W. Richardson, M. B. Tsang, R. E. Ellis, and C. K. Gelbke, Phys. Lett. **108B**, 274 (1982).
[24]C. B. Chitwood, D. J. Fields, C. K. Gelbke, D. R. Klesch, W. G. Lynch, M. B. Tsang, T. C. Awes, R. L. Ferguson, F. E. Obenshain, F. Plasil, R. L. Robinson, and G. R. Young, Phys. Rev. C **34**, 858 (1986).
[25]B. A. Remington, G. Caskey, A. Galonsky, C. K. Gelbke, L. Heilbronn, J. Heltsly, M. B. Tsang, F. Deak, A. Kiss, Z. Seres, J. Kasagi, and J. J. Kolata, Phys. Rev. C **34**, 1685 (1986).
[26]F. Deak, A. Kiss, Z. Seres, G. Caskey, A. Galonsky, C. K. Gelbke, B. Remington, M. B. Tsang, and J. J. Kolata, Nucl. Phys. **A464**, 133 (1987).
[27]D. Fox, D. A. Cebra, J. Karn, C. Parks, A. Pradhan, A. Vander Molen, J. van der Plicht, G. D. Westfall, W. K. Wilson, and R. S. Tickle, Phys. Rev. C **38**, 146 (1988).
[28]D. A. Cebra, W. Benenson, Y. Chen, E. Kushy, A. Pradhan, A. Vander Molen, G. D. Westfall, W. K. Wilson, D. J. Morrissey, R. S. Tickel, R. Korteling, and R. Helmer, Phys. Lett. B **227**, 336 (1989).
[29]H. Delagrance and J. Peter, Nucl. Phys. **A471**, 111c (1987).
[30]D. Fabris *et al.*, Nucl. Phys. **A471**, 351c (1987).
[31]R. Wada *et al.*, Phys. Rev. C **39**, 497 (1989).
[32]R. E. L. Green, R. G. Korteling, and K. P. Jackson, Phys. Rev. C **29**, 1806 (1984).
[33]R. E. L. Green, R. G. Korteling, J. M. D'Auria, K. P. Jackson, and R. L. Helmer, Phys. Rev. C **35**, 1341 (1987).
[34]R. E. L. Green, D. H. Boal, R. L. Helmer, K. P. Jackson, and R. G. Korteling, Nucl. Phys. **A405**, 463 (1983).
[35]R. L. Helmer, R. E. L. Green, K. P. Jackson, and R. G. Korteling, Phys. Rev. C **29**, 676 (1984).
[36]R. E. L. Green and R. G. Korteling, Phys. Rev. C **22**, 1594 (1980).
[37]R. E. L. Green and R. G. Korteling, Phys. Rev. C **18**, 311 (1978).
[38]K. Kwiatkowski, J. Bashkin, H. Karwowski, M. Fatyga, and V. E. Viola, Indiana Cyclotron Report INC-40007-30, 1985 (unpublished).
[39]D. H. Boal, R. E. L. Green, R. G. Korteling, and M. Soroushin, Phys. Rev. C **23**, 2788 (1981).
[40]D. H. Boal, in Proceedings of the Relativistic Heavy Ion Winter School Banff, 1982, TRIUMF Report TRI-PP-82-7, 1982 (unpublished).
[41]R. E. L. Green, K. P. Jackson, and R. G. Korteling, Phys. Rev. C **25**, 828 (1982).
[42]D. H. Boal and J. H. Reid, Phys. Rev. C **29**, 973 (1984).
[43]J. B. Cumming, P. E. Haustein, T. J. Ruth, and G. J. Virtes, Phys. Rev. C **17**, 1632 (1978).
[44]D. H. Boal and J. N. Glosli, Phys. Rev. C **38**, 1870 (1988); **38**, 2621 (1988).
[45]D. H. Boal, J. N. Glosli, and C. Wicentowich, Phys. Rev. Lett. **62**, 737 (1989).

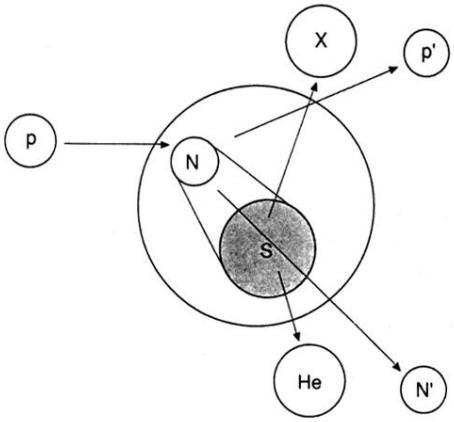

FIG. 21. Schematic proton-induced fragmentation reaction. *N* Represents a nucleon, *X* an unknown partner to the emitted He fragment, and *S* the fragment emitting source.